Journal of Marine Science and Technology

Volume 24 | Issue 4 Article 19

WINTER SEA FOG DETECTION USING TRMM MICROWAVE MEASUREMENTS OVER THE TAIWAN STRAIT

Nan-Ching Yeh
Department of Aircraft Engineering, Air Force Institute of Technology, Kaohsiung, Taiwan, R.O.C,
jim912104@gmail.com

Wann-Jin Chen
College of Living and Health Technology, Ta Hwa University of Science and Technology, Hsinchu, Taiwan, R.O.C.

Gin-Rong Liu
Center for Space and Remote Sensing Research, National Central University, Taoyuan, Taiwan, R.O.C.

Chung-Chih Liu
Minghsin University of Science and Technology, Hsinchu, Taiwan, R.O.C.

Journal of Marine Science and Technology, Vol. 24, No. 4, pp. 851-863 (2016)
DOI: 10.6119/JMST-016-0429-1

WINTER SEA FOG DETECTION USING TRMM MICROWAVE MEASUREMENTS OVER THE TAIWAN STRAIT

Nan-Ching Yeh[1], Wann-Jin Chen[2], Gin-Rong Liu[3], and Chung-Chih Liu[4]

Key words: fog detection, microwave brightness temperature, fog observations, polarization TB.

ABSTRACT

The impact of fog on activities such as land transportation, flight and marine operations, and military missions can be dangerous. Thus, this study developed a new and simple method for detecting fog areas over the Taiwan Strait more accurately during winter by using the Tropical Rainfall Measuring Mission Microwave Imager (TMI) Level-1B calibrated brightness temperature (TB) data, combined with ground station fog observations. This method is based on the microwave TB differences among four TMI channels, including horizontal and vertical polarization TBs of 37.0 and 85.5 GHz, for heavy fog and clear weather conditions. The method can be applied to large areas during the daytime and nighttime and distinguish fog from low clouds. It involves selecting fog cases and recognizing fog areas, removing relevant land data and calculating TMI TB statistics, establishing TB fog criteria, and finally validating the fog criteria through analysis of independent cases. The results indicated that the fog detection accuracy reached 75%. Among the four channels of the TMI, the 85.5 GHz horizontal polarization exhibited the highest fog sensitivity.

I. INTRODUCTION

In addition to the large number of vessels that pass through the Taiwan Strait, many airplanes fly across the Strait each day. According to statistics from the MINISTRY OF TRANSPORTATION AND COMMUNICATIONS R.O.C. (MOTC), 2.5 million and 2.6 million people flew to the outlying Taiwan-controlled islands located in the Taiwan Strait during 2013 and 2012, respectively. The fog over Taiwan occurs most frequently during winter. Therefore, as implied by the aforementioned maritime and aviation statistics, fog detection over the Taiwan Strait during winter is critical.

According to the World Meteorological Organization (WMO), when fog is present, horizontal visibility is lower than 1000 m. Gultepe et al. (2014) demonstrated that the respective visibility for heavy ice fog, intermediate ice fog, and light ice fog is lower than 1000 m, between 1000 and 5000 m, and higher than 5000 m. When visibility is less than 500 m at sea or in the air, or less than 200 m on land, the Central Weather Bureau of Taiwan issues a heavy fog warning to the public. Cho et al. (2000) observed a high frequency of sea fog occurrence (more than 50%) when the dew point exceeded 285 K and the difference between the dew point and sea surface temperature was typically more than 2 K, according to a decade of observations around the Korean peninsula. Pagowski et al. (2004) revealed that the forecasting of fog is considerably difficult because of its high variability and the complicated physical processes that occur in the boundary layer. Gultepe et al. (2007a) indicated that the complex fog processes involve droplet microphysics, aerosol chemistry, radiation, turbulence, and large-scale and small-scale dynamics, and are influenced by the types of surface condition. They demonstrated that the liquid water content, droplet concentration, and droplet size increase during the formation of fog. Kim and Yum (2010) observed that the formation of cold sea fog over the Yellow Sea off the west coast of the Korean peninsula was relative to the movement of moist and warm air over the cold surface. Kim and Yum (2011) indicated that turbulent cooling and radiative cooling occurred before the onset of fog, thus crucially contributing toward decreasing temperature over the cold surface and to the water vapor saturation in the boundary layer.

Two methods are typically used to observe fog: (1) physical observation without the use of instruments, and (2) observation using a visibility meter. However, these two approaches cannot satisfy the current information demand for fog detection because of their limited spatial coverage over both land and sea. Nevertheless, this downside can be overcome by using

Paper submitted 12/06/14; revised 05/15/15; accepted 04/29/16. Author for correspondence: Nan-Ching Yeh (e-mail: jim912104@gmail.com).
[1] *Department of Aircraft Engineering, Air Force Institute of Technology, Kaohsiung, Taiwan, R.O.C.*
[2] *College of Living and Health Technology, Ta Hwa University of Science and Technology, Hsinchu, Taiwan, R.O.C.*
[3] *Center for Space and Remote Sensing Research, National Central University, Taoyuan, Taiwan, R.O.C.*
[4] *Minghsin University of Science and Technology, Hsinchu, Taiwan, R.O.C.*

satellite observations. In general, infrared (IR) and visible (VIS) satellite data can be used for fog detection. Eyre et al. (1984) used the brightness temperature (TB) difference between two IR window channels to detect fog. The detection method is based on the different thermal emissivity of fog from the two IR channels. Several subsequent studies (Wetzel et al., 1996; Lee et al., 1997; Anthis and Cracknell, 1999; Greenwald and Christopher, 2000; Bendix, 2002) have employed similar techniques. The techniques involve the use of TB differences observed from the 3.9 (3.7) μm and 11.2 (11.0) μm channels from Geostationary Operational Environmental Satellites (National Oceanic and Atmospheric Administration Advanced Very High Resolution Radiometer). Another approach entails using the TB difference between the IR4 (3.5-4 μm) and IR1 (10.3-11.3 μm) from the Multifunctional Transport Satellites (MTSAT). However, this approach can be used only at night, when no reflected solar radiation is present to affect the TB of the shortwave channels (Bader et al., 1995).

In recent years, various fog detection studies using satellite data have been conducted. Gultepe et al. (2007b) indicated that satellite observations cannot be used for accurate fog detection when VIS channels are not available (i.e., during nighttime). Liu and Hu (2008) established a series of thresholds for fog detection by using MTSAT data; however, the method can be used only during the daytime. Gao et al. (2009) demonstrated that the TB difference between the shortwave and longwave ranging from -5.5°C to 2.5°C can be used as a criterion for determining the area of sea fog over the Yellow Sea. Thresholds of TB and albedo for fog detection, which greatly improved sea fog detection, were derived by Yoo et al. (2010). Bendix et al. (2006) and Cermak and Bendix (2008) have developed methods for detecting fog and low stratus clouds during the daytime, but with no differentiation. In addition, Cermak and Bendix (2011) developed a technique for distinguishing low stratus clouds and fog on the basis of METEOSAT Second Generation Spinning-Enhanced Visible and Infrared Imager data. However, this technique can be used only during the daytime. Thus, some methods have been devised to detect sea fog, but are limited to either daytime or nighttime use. Wang et al. (2014) attempted to overcome this limitation by developing a method that can detect sea fog for both day and night by using a combination of the various methods proposed by previous studies. However, the principal method for detecting fog during the daytime still differed from the approach that was used for nighttime conditions. Evidently, despite the substantial research that has been performed on fog detection methods, additional improvements are required. Although the combined use of two IR channels, such as 3.9 (3.7) and 11.2 (11) μm, enables detecting fog, this approach is limited to nighttime cases (Bader et al., 1995). Furthermore, Eric et al. (1997) indicated that if fog is present at night, it may remain undetected because there are no available VIS images. A simple method for detecting fog during both the daytime and nighttime and distinguishing it from low clouds seems to be lacking. Hamazu et al. (2003) indicated that the vertical attenuation in fog is relatively weak compared with the horizontal attenuation; therefore, high frequency channels are the most appropriate for vertical observations in airborne or satellite-borne applications. The main purpose of our study was to establish a novel method for detecting fog during winter over the Taiwan Strait by using four high frequency Tropical Rainfall Measuring Mission (TRMM) Microwave Imager (TMI) channels during both the daytime and nighttime. Using a combination of the method proposed in this study and the IR detection method enables reduction of fog-induced aviation and sea disasters.

The collection of TMI and MTSAT data and relevant ground observations is discussed in Section 2. Section 3 describes the methodology regarding foggy area recognition, case selection, and research processing. In Section 4, the results from an independent case verification are presented and discussed. Finally, Section 5 concludes the study with comments on the developed method for fog detection, its limitations, and future work.

II. THEORETICAL BASIS

The typical fog particle size (0.5-40 μm) is approximately 1 μm, and the typical cloud particle size (10-100 μm) is greater than 10 μm. Theoretically, the liquid water content of fog is 0.1 gm^{-3}, whereas that of clouds is greater than 0.4 gm^{-3} (Wang, 1997). Fog, clouds, and rain differ in their liquid water content. In other words, fog can be considered either a cloud or a type of rainfall, depending on perspective.

In the spectral range of the IR window channels, most of the radiation measured by satellites is emitted by surfaces such as from land, sea, and cloud tops. Because atmospheric absorption is relatively light within these window channels, they can be used to observe surfaces during the absence of clouds. Fog can be detected by analyzing the variation of the emissivity from two IR channels. Specifically, the effective temperature of fog at 3.7/3.9 μm is lower than at 11/11.2 μm, but the temperature of both land and sea monitored through these channels is approximately the same. Therefore, the TB difference between two IR channels is sensitive to the presence of fog or low stratiform clouds.

Eric et al. (1997) indicated that individual cloud types can be identified by observing various cloud features including the brightness, edge definition, texture, size, organizational pattern, and individual shape in a VIS satellite image. In IR and VIS images, fog and stratiform clouds are characterized by smooth and flat tops, a lack of an organized pattern, and, typically, sharp boundaries. In satellite image animations, clouds generally move with the upper winds while fog remains stationary. Bader et al. (1995) reported that fog can often be detected using IR image enhancement and image animation. Generally, using VIS and IR images simultaneously enables accurately detecting the location of fog areas.

The most effective method for recognizing cloud types involves acquiring VIS and IR images of the same location. In a VIS image, fog appears to have a smooth flat texture. In an

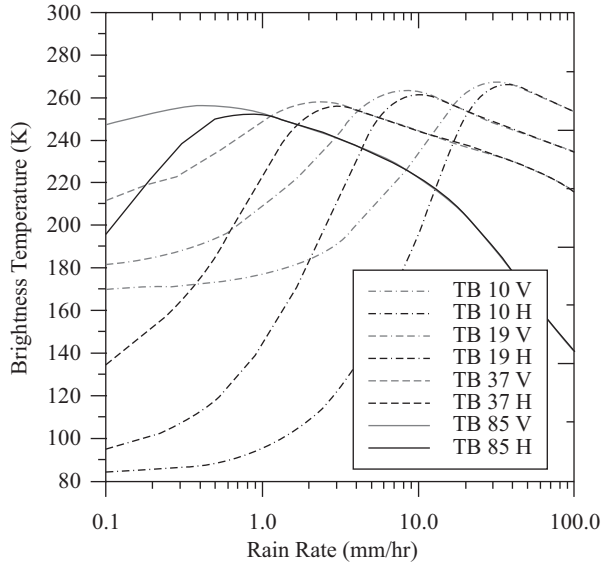

Fig. 1. Relationship between TB and surface rainfall rate over the ocean for TMI channels of 10, 19, 37, and 85 GHz in the standard atmosphere (Hu et al., 2009).

IR image, fog exhibits a gray shade. Relying on these features alone renders distinguishing fog from stratiform clouds difficult. Eric et al. (1997) demonstrated that when multiple or time-lapse images are available, a useful rule of thumb is that if a cloud with a smooth flat texture and gray shade does not move, it is generally fog.

Hu et al. (2009) detailed the relationship between the TB and the rainfall rate (RR) over the ocean in a standard atmosphere (Fig. 1) when horizontal homogeneity of rain clouds is assumed. When it rains, the TB in all channels increases with the RR because of emissions from the cloud water and rain water. By contrast, beyond a certain saturation point, the TB decreases with the increasing RR because of more significant scattering. Fig. 1 illustrates that the saturation point reaches faster at a higher microwave frequency than at a lower frequency. Therefore, the drop in the TB caused by scattering is more substantial at lower frequencies than at higher frequencies. Gultepe et al. (2009) demonstrated that the liquid water content increases with the droplet number concentration (Nd). The preceding discussion indicates that the microwave TB and liquid water content are directly proportional. Therefore, the droplet number concentration is directly proportional to the microwave TB before microwave channel saturation.

Regarding RR retrieval, because lower frequency of TMI has a stronger relationship with the RR and a wider dynamic range than higher frequency channel, retrieval of stratiform rainfall is typically performed with low frequency data. By contrast, the TB observed using higher frequency channels reaches saturation when the RR is greater than 3 mm hr^{-1} (Petty et al., 2001). However, the scattering effects caused by larger raindrops or solid precipitation are more significant at a higher frequency of TMI.

Satellite passive microwave observation is widely used for rainfall estimation over the ocean (Adler et al., 2001). Employing passive microwaves to estimate the RR entails using the emission effects of liquid water observed from channels lower than 30 GHz before saturation. Conversely, when the estimation involves larger raindrops or solid precipitation, the scattering effects observed from channels higher than 60 GHz after saturation are used instead (Petty et al., 2001). Fig. 1 illustrates that the slopes of the higher frequency (37 GHz and 85 GHz) channels are steeper than those of other channels (10 GHz and 19 GHz) before the saturation of all channels (probably less than 0.7 mm hr^{-1}), especially for the horizontal polarization of a higher frequency. Consequently, the horizontal polarization of a higher frequency should be more sensitive to fog before the saturation of all TMI channels. This will be further verified in Section 5.

As mentioned, the liquid water content of fog is less than that of clouds or rain. Therefore, satellite passive microwaves can be used to detect fog according to the emission effects at higher frequencies, which are generally unavailable for rainfall estimations.

III. DATA COLLECTION

1. TMI Satellite Data

The TRMM satellite was launched in 1997. The TMI was a passive microwave sensor onboard the TRMM satellite that scans the earth conically with a swath of 878 km and an incident angle relative to the ground surface of approximately 52.8°. The TMI measures the radiation intensity at five frequencies: 10.65, 19.35, 21.3, 37.0, and 85.5 GHz. The 21.3 GHz frequency has only vertical polarization, but the other four frequencies have dual polarization. The field of view (FOV) of the TMI depends on the frequency. The data used in this study are a Level-1B11 product, which has already undergone radiation correction and geometric positioning. The product has a spatial resolution of 10 km. For convenience, the vertically polarized TBs in the TMI channels are denoted as T_{10V}, T_{19V}, T_{21V}, T_{37V}, and T_{85V}; where V represents vertical polarization and H represents horizontal polarization.

2. MTSAT Satellite Data

The MTSAT 1R (MTSAT-IR) is a geostationary satellite that was launched into orbit 35 800 km above the equator at the longitude of 140°E in 2005. The MTSAT-1R has five channels: one VIS channel, two IR channels, one water vapor channel, and one near-IR channel. The spatial resolution for the visible channel is 1 km, whereas it is 4 km for all other channels. Both IR and VIS images were used in this study.

3. Ground Station Observations (Beigan and Magong Airports)

Ground station observations from the Beigan and Magong airports during the winters of 2006-2010 were provided by the Aviation Weather Center of the Civil Aeronautics Admini-

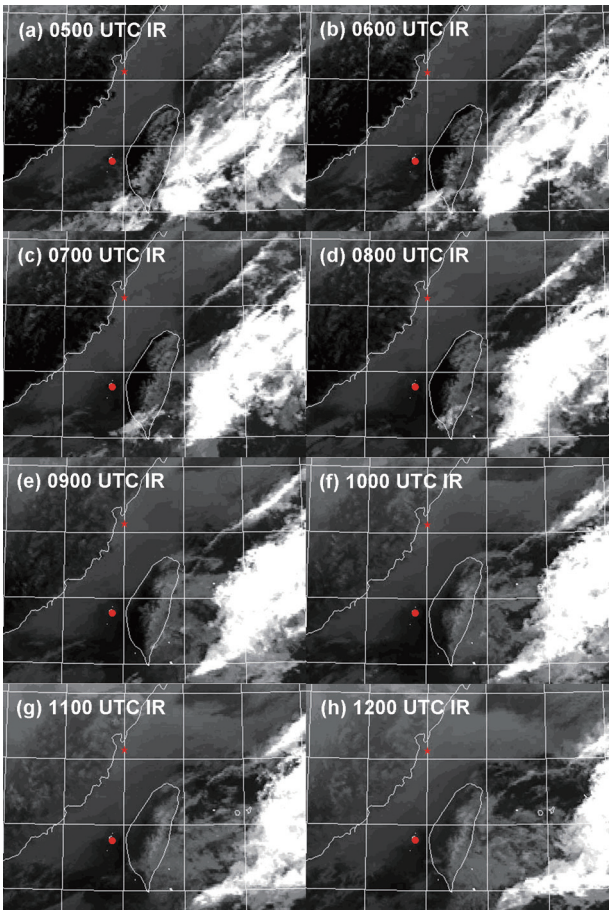

★: Beigan airport, •: Magong airport

Fig. 2. MTSAT IR observations at (a) 0500, (b) 0600, (c) 0700, (d) 0800, (e) 0900, (f) 1000, (g) 1100, and (h) 1200 UTC on January 16, 2006.

stration and the Meteorological Center of the Republic of China Air Force, respectively. The two airports are located at 26°13'N, 120°00'E and 23°34'N, 119°37'E, respectively. The datasets include temperature, the dew point, wind direction and speed, and visibility data. For this study, only the visibility data were employed.

IV. METHODOLOGY

1. Recognizing Fog

The first step in processing our data was to differentiate fog events from cloudy weather. This was performed by examining both IR and VIS image animations. As theoretical studies have mentioned, the combination of VIS and IR images can be used to locate fog areas. IR images capture the amount of longwave radiation from the cloud surface or ground surface, including sea and land surfaces. In addition, fog generally appears close to the land or sea surface. Thus, in IR images, the TB of fog is only slightly different compared with that of the land or sea surface.

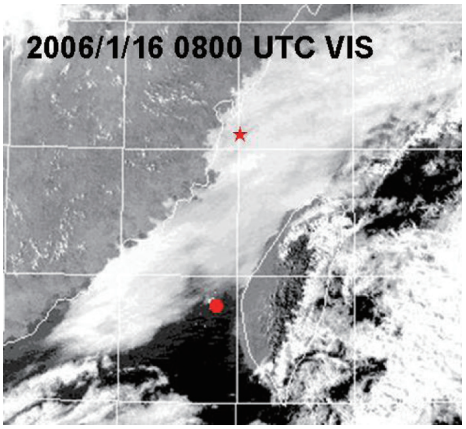

★: Beigan airport, •: Magong airport

Fig. 3. MTSAT VIS observation at 0800 UTC on January 16, 2006.

Fog events were selected by analyzing the TBs from IR images, albedo from VIS images, and cloud movement from successive satellite images. Each selected fog event was further verified according to visibility reports from airports situated within the region. Fig. 2 provides an example. Figs. 2(a)-(h) illustrate a series of MTSAT-1R IR images from 0500 to 1200 UTC, and Fig. 3 depicts a VIS image from 0800 UTC on January 16, 2006. As mentioned, fog regions can be distinguished from clouds by using satellite image animation, because clouds move with the winds, whereas the movement of fog is minimal for several hours. The images in Fig. 2 show that the clouds located in the waters east of Taiwan evidently moved eastward. By contrast, the fog areas in the Taiwan Strait remained stationary for approximately 7 hours. Another key characteristic of fog is that it has a higher albedo than clear skies. Fig. 3 illustrates that the albedo over the Taiwan Strait is higher than that in the clear skies near the coastal waters of southwest Taiwan.

By using the series of IR and VIS images displayed in Figs. 2 and 3, the target region located in the Taiwan Strait was verified to satisfy the criteria for fog, indicating that a fog event was highly probable. Further evidence was provided by the Beigan airport observations, which showed that the visibility was 400 m at 0800 UTC. The Beigan airport is located in the Taiwan Strait, which is inside the target region.

2. Selection of Cases

Because the primary goal of this study was to detect fog events over the Taiwan Strait during winter, cases were selected by identifying low visibility observations made by the Beigan and Magong airports. The selected TMI satellite observations corresponded to the period when the fog reports were made.

3. Research Process

A flowchart that summarizes our research method is presented in Fig. 4. Our proposed fog detection process consisted of four steps described as follows:

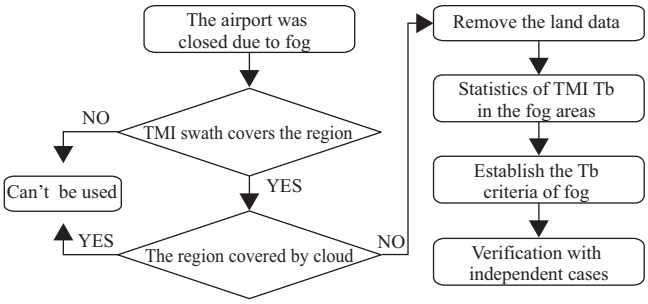

Fig. 4. Research process flowchart for fog detection.

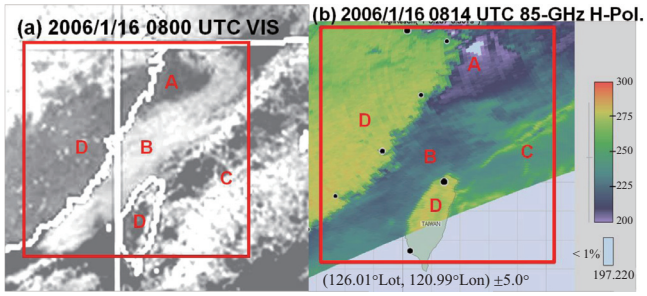

Fig. 5. (a) Clear sky areas (A), fog areas (B), cloud areas (C), and land areas (D) in the MTSAT VIS observation at 0800 UTC on January 16, 2006, (b) same as (a), but 85 GHz horizontal polarization TB image of TMI at 0814 UTC.

Step 1: Selecting Fog Cases and Recognizing Fog Areas

Fig. 5(a) depicts a VIS image from 0800 UTC on January 16, 2006. Fig. 5(b) illustrates the TMI 85 GHz horizontal polarization TB at 0814 UTC on January 16, 2006, where the color bar indicates the TB value. Clear skies, fog, clouds, and land are present within the red square region in Fig. 5 and are marked respectively as A, B, C, and D. Fig. 5(b) shows that the land regions had the highest TB, as indicated by the emissivity being the highest in the microwave region. Contrarily, the ocean regions with clear skies had the lowest TB; this was indicated by the emissivity being the lowest in the microwave region. The TBs of the clouds and fog were between the maximum and minimum TBs, but the TBs of the clouds were higher than those of the fog, because of a higher liquid water content.

Fig. 6 shows a histogram depicting the distribution of the microwave data within the red square in Fig. 5. Fig. 6 has four peak values, marked as A, B, C, and D, further illustrating the viability of using passive microwave data in detecting fog. Conventionally, passive microwave data are used to estimate various physical parameters such as the rain rate, sea surface temperature, sea surface wind field, and air-sea energy fluxes. Fog detection is a novel research topic. In this study, the chosen fog areas encompassed a region from 23.0°N to 27.5°N and 117.0°E to 122.1°E at 0800 UTC on January 16, 2006, and from 23.2°N to 26.0°N and 117.2°E to 121.5°E at 0300 UTC on February 3, 2009. The corresponding diagrams are depicted in Fig. 7.

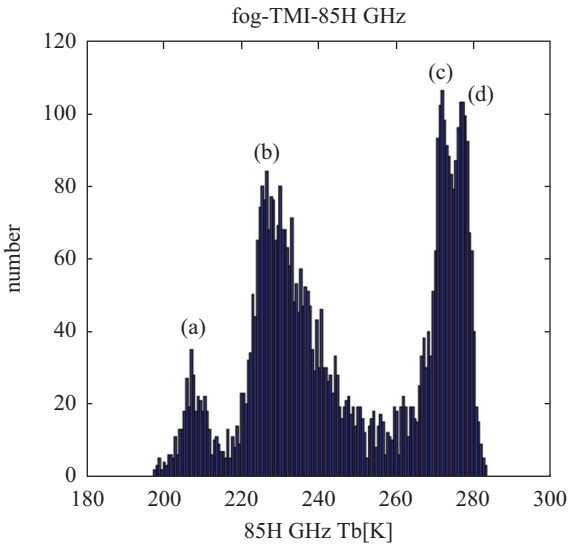

Fig. 6. Histogram of TBs of clear sky areas (a), fog areas (b), cloud areas (c), and land areas (d) shown in Fig. 5(b).

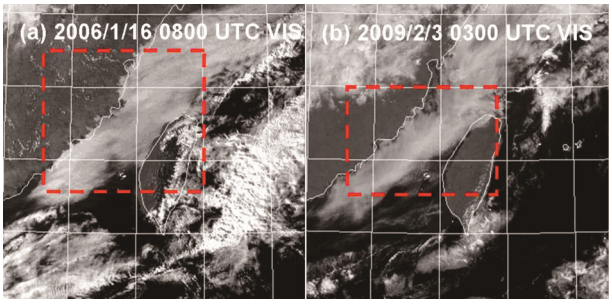

Fig. 7. MTSAT-1R VIS observations at (a) 0800 UTC on January 16, 2006; and (b) at 0300 UTC on February 3, 2009. Dashed lines show the chosen fog areas.

Step 2: Removing the Land Data and Calculating the TMI TB Statistics

This step involves removing the land data and calculating the TMI TB mean value (μ) and standard deviation (σ) of the fog areas that were selected in Step 1. The land data are removed when the TMI observations include land surfaces or areas that are within 20 km of land. The purpose of data deletion is to prevent the high emissivity of land surfaces from affecting data retrieval over the ocean. The TB histograms of the four channels are illustrated in Fig. 8. For each channel, the distribution was similar to a Gaussian distribution. After the removal of the land data, the red square region in Fig. 7 mostly consisted of fog and contained only a few sporadic areas with clouds or clear skies. This lack of clouds and clear skies explains why there is a scant amount of extreme outliers in Fig. 8. These outliers, which were not within the range ($\mu + 2\sigma$, $\mu - 2\sigma$), were discarded in this study. The results, with a 95% confidence level, are depicted in Fig. 9. The μ and σ

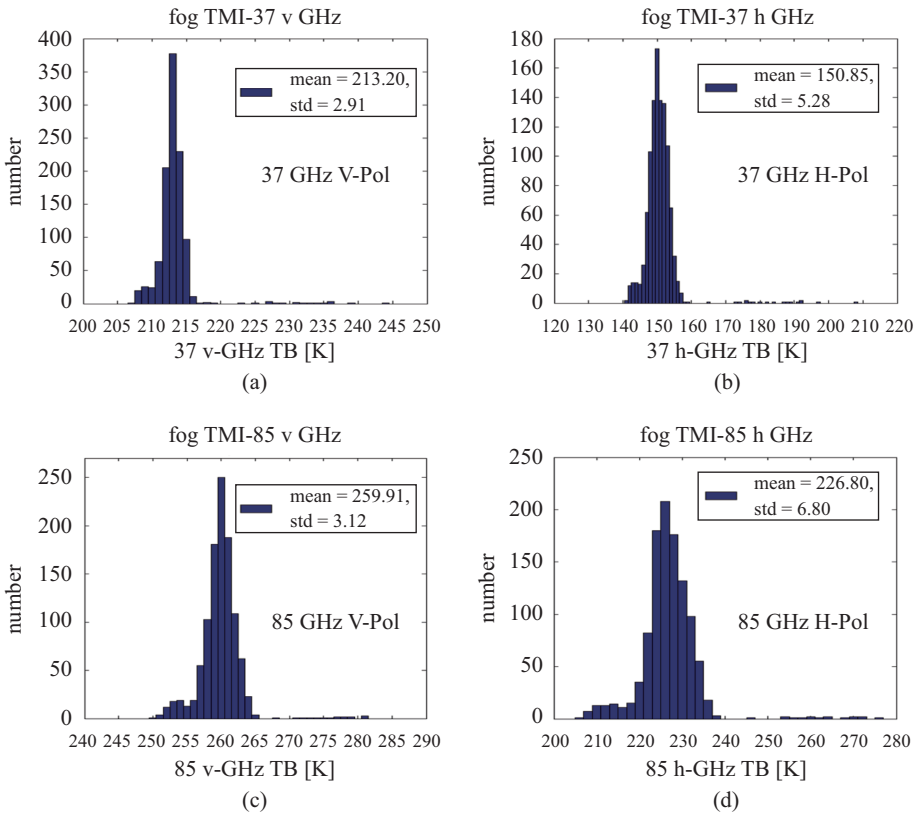

Fig. 8. TB histograms of the four TMI channels within the selected range shown in Fig. 7.

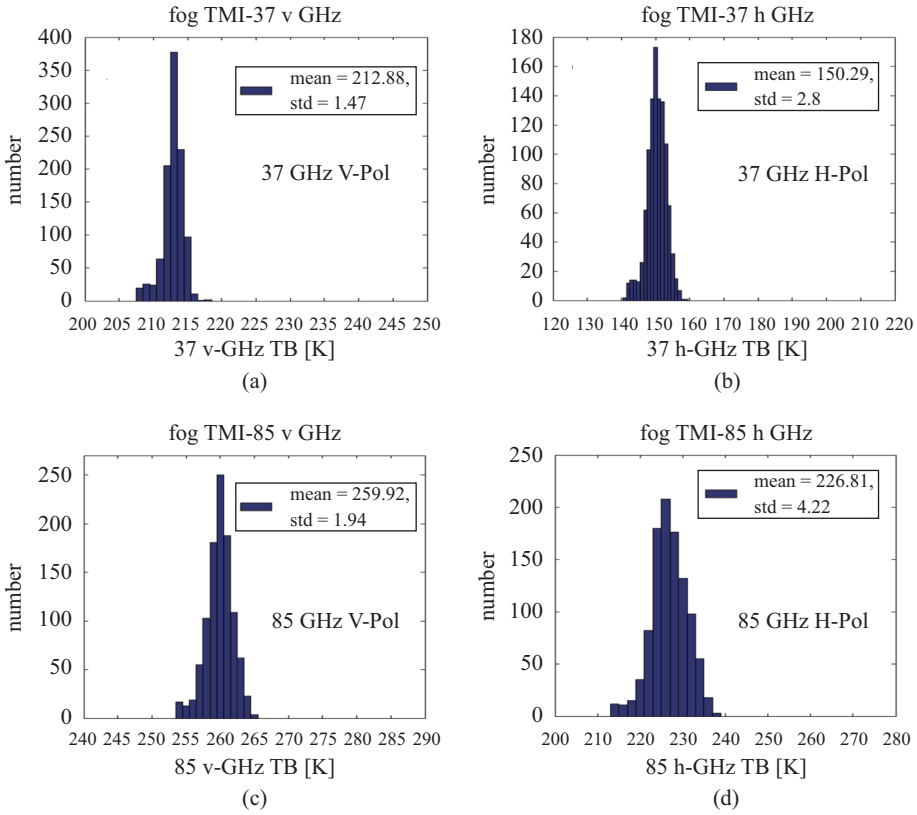

Fig. 9. TB histograms of the four TMI channels for fog.

Table 1. Mean and standard deviation values of TB of the four TMI channels for fog.

Channels	mean value	standard deviation
TB37 V	212.9 K	1.47
TB37 H	150.3K	2.8
TB85 V	259.9K	1.94
TB85 H	226.8K	4.22

Table 2. Four criteria for fog.

Channels	criteria ((μ - 2σ) ~ (μ + 2σ))
TB37 V	209.9 K ~ 215.8 K
TB37 H	144.7 K ~ 155.9 K
TB85 V	256.0 K ~ 263.8 K
TB85 H	218.4 K ~ 235.3 K

Table 3. Ten cases of fog.

Case	Date	Time (UTC)	Orbit Number	Airport	Visibility
1	2006/1/31	00:54	46791	Beigan	100 m at 0:00
					0 m at 01:00
2	2006/1/31	00:54	46791	Magong	1000 m at 0:00
					2800 m at 01:00
3	2006/2/15	22:08	47039	Magong	400 m at 22:00
					400 m at 23:00
4	2007/2/8	09:29	52610	Beigan	700 m at 09:00
					700 m at 10:00
5	2007/2/9	03:40	52622	Beigan	2100 m at 03:00
					600 m at 04:00
6	2007/2/9	08:33	52625	Beigan	900 m at 08:00
					900 m at 09:00
7	2008/1/11	00:38	57857	Beigan	800 m at 0:00
					500 m at 01:00
8	2008/1/11	23:43	57872	Beigan	1800 m at 23:00
					600 m at 24:00
9	2009/2/11	21:34	64058	Beigan	300 m at 21:31
					300 m at 22:00
10	2010/2/23	22:15	69935	Magong	1200 m at 22:00
					400 m at 22:30

values of TB for fog areas observed from the four channels are presented in Table 1.

Step 3: Establishing the TB Criteria for Fog

The TB criteria for fog observed from the four channels can be established once the average TB values and standard deviations of the fog areas are established in Step 2. The criteria of the four channels range from (μ - 2σ) to (μ + 2σ), and are summarized in Table 2.

Table 4. Ten cases of nonfog (including clear and cloudy skies).

Case	Date	Time (UTC)	Orbit Number	Airport	Visibility
11	2006/1/12	09:41	46501	Beigan	5000 m at 09:00
					5000 m at 10:00
12	2006/2/15	22:08	47039	Beigan	1200 m at 22:00
					1200 m at 23:00
13	2007/2/8	09:29	52610	Magong	8000 m at 09:00
					8000 m at 10:00
14	2008/1/11	23:43	57872	Magong	3200 m at 23:00
					4800 m at 24:00
15	2008/1/11	00:38	57857	Magong	4800 m at 00:00
					7000 m at 01:00
16	2009/1/11	06:56	63566	Beigan	10000 m at 06:00
					10000 m at 07:00
17	2009/1/11	06:56	63566	Magong	9999 m at 06:00
					9999 m at 07:00
18	2009/1/26	22:43	63810	Beigan	6000 m at 22:00
					6000 m at 23:00
19	2009/1/26	22:43	63810	Magong	9999 m at 22:00
					9000 m at 23:00
20	2009/2/11	21:34	64058	Magong	2100 m at 21:00
					1200 m at 22:00

Step 4: Verification with Independent Cases

After the fog detection criteria are established, they must be verified according to independent cases. The verification was based on a quantitative analysis of 20 independent cases that had occurred during January and February from 2006 to 2010, which comprised 10 fog cases and 10 nonfog cases. The nonfog cases included cloudy and clear skies. Table 3 and Table 4 respectively list the quantitative results for fog cases and nonfog cases. Four independent weather conditions were used for the qualitative analysis. The first and second conditions were fog cases that had occurred respectively on February 8, 2007, and January 31, 2006. The third was a clear weather case recorded on January 11, 2009, and the fourth condition was a cloud case that occurred on January 26, 2009.

V. RESULTS AND DISCUSSION

This section describes the qualitative and quantitative validation of fog detection. First, we present a qualitative comparison of the horizontal structures from TMI observations, comprising two fog cases and two nonfog cases. This comparison was conducted mainly against IR and VIS observations. Because the coverage of the TMI observations in the Taiwan Strait is not fixed, each swath within the validation area (Taiwan Strait) exhibits a variation of approximately 1000 m in the FOV. Therefore, our comparison involved approximately 4000 verification cases. Second, we present quantitative comparisons

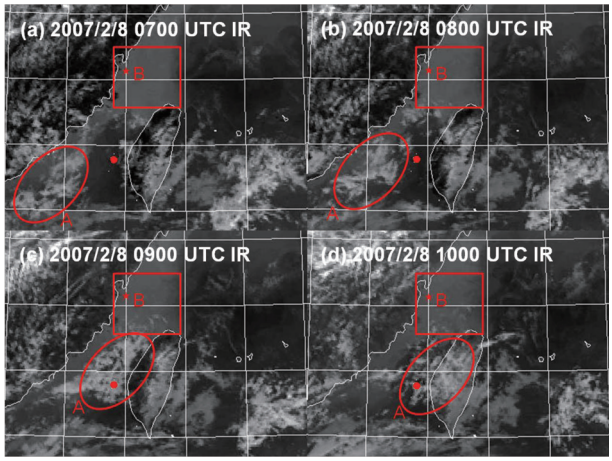

★: Beigan airport, •: Magong airport

Fig. 10. MTSAT IR observations at (a) 0700, (b) 0800, (c) 0900, and (d) 1000 UTC on February 8, 2007.

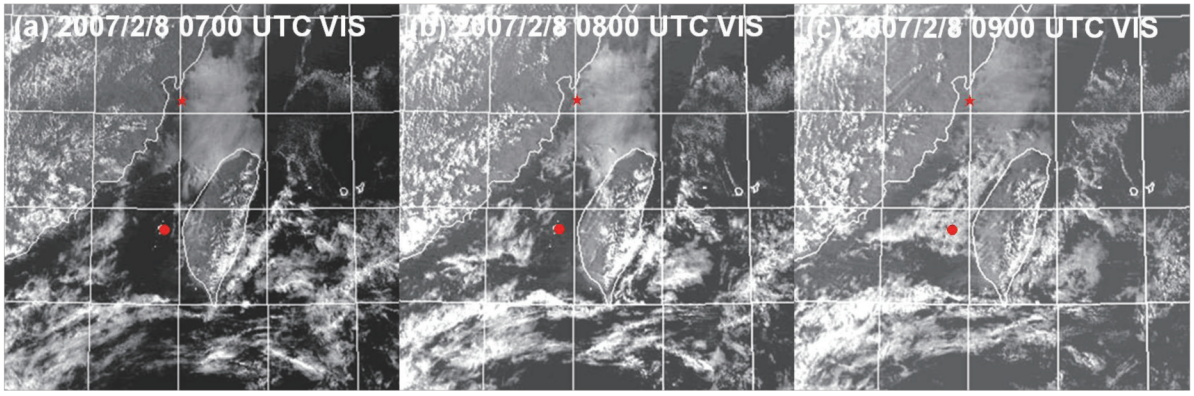

★: Beigan airport, •: Magong airport

Fig. 11. MTSAT VIS observations at (a) 0700, (b) 0800, and (c) 0900 UTC on February 8, 2007.

against the ground station observations from two airports. Currently, this is the only viable means for quantitatively validating fog over the Taiwan Strait. This is because the TRMM satellite is no geostationary, and the TMI instrument scans the area around Taiwan two or three times per day. Even when the swath of the TMI is in the vicinity of Taiwan, it does not necessarily cover the entire Taiwan Strait. Furthermore, the airport must have fog when the swath of the TMI covers the Taiwan Strait. Therefore, it was very difficult to identify cases for quantitative validation. In this study, we selected 20 independent cases during the winter of 2006-2010 for quantitative validation.

1. Qualitative Analysis

1) Fog Cases

The first case was a fog condition. The TMI scan time was 0929 UTC on February 8, 2007, and the TRMM orbit number was 52610. Figs. 10(a)-(d) depict a series of MTSAT IR observations from 0700 to 1000 UTC on this day. There were two distinct TBs from the cloud top in the Taiwan Strait during this period. One was from the south and middle parts of the Taiwan Strait, and was moving northeastward toward central Taiwan (region A). The other was from the northern Taiwan Strait and remained stationary (region B). Figs. 11(a)-(c) illustrate a series of MTSAT VIS observations from 0700 to 0900 UTC on February 8, 2007. The target in the northern Taiwan Strait had a higher albedo than that of a clear sky and thus exhibited a smooth appearance in the VIS image. Conversely, the target in the south and middle parts of the Taiwan Strait exhibited cloud textures. The IR and VIS images in Figs. 10 and 11 provide information for distinguishing the target in the south and middle parts of the Taiwan Strait as clouds, and the target in the northern Taiwan Strait as fog.

The fog detection results are presented in Fig. 12. Figs 12(a)-(c) depict the results obtained when more than one, two, and three fog criteria were met, respectively; Fig. 12(d) depicts the outcome when all four fog criteria were satisfied. The circles in Fig. 12 depict the foggy areas and represent the FOV of the TMI. Analysis of the fog criteria in Fig. 12 suggests that a

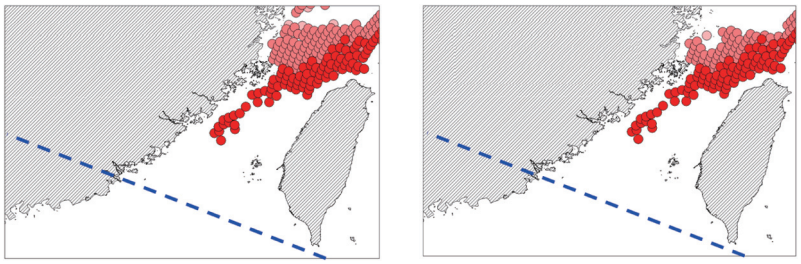

(a) Meet more than one criterion (b) Meet more than two criteria

(c) Meet more than three criteria (d) Meet four criteria

Fig. 12. Case verification at 0929 UTC on February 8, 2007. The figures meet more than (a) one, (b) two, (c) three criteria, and (d) all four criteria. Dashed line delineates the edge of swath, and the purple circles indicate the FOV of TMI.

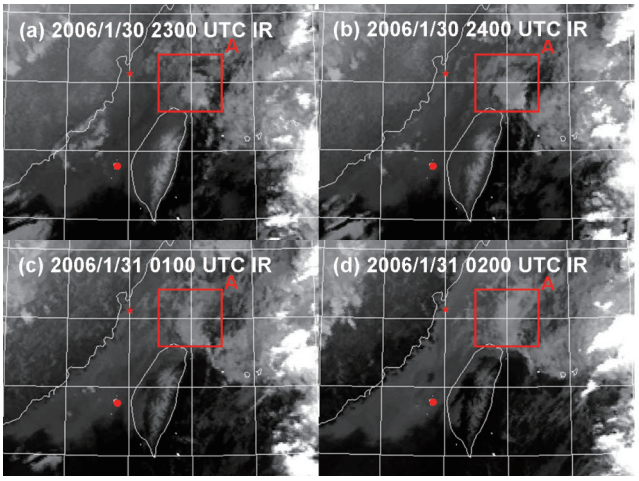

★: Beigan airport, •: Magong airport

Fig. 13. MTSAT IR observations at (a) 2300 UTC on January 30, 2006; and (b) 0000, (c) 0100, and (d) 0200 UTC on January 31, 2006.

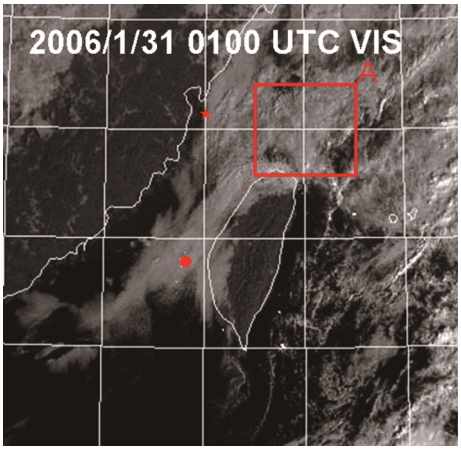

Fig. 14. MTSAT VIS observation at 0100 UTC on January 31, 2006.

significant sea fog area was located north of the Taiwan Strait, which is consistent with the satellite observations. Final verification was conducted using visibility reports that covered the particular regions.

Figs. 12(a)-(c) indicate that sea fog existed within 20 km of the Beigan airport. The sea fog area grew smaller near the Beigan airport when all four fog criteria were met, as illustrated in Fig. 12(d). In addition, Fig. 12(a) shows that no sea fog area existed near the Magong airport, as indicated by only one fog criterion being satisfied. The ground truth observations from the isolated islands in the Taiwan Strait were applied to verify the derived results. The ground station observations from the Beigan airport showed that the visibility was only 700 m, and the Magong airport reported an 8000 m visibility at that time. This information provides an example of accurate detection. The circles in Fig. 12 represent the fog areas. Conversely, the absence of circles indicates that the visibility should have been more than 1000 m.

The second case was also a fog condition. The TMI scan time was 0054 UTC on January 31, 2006, and the TRMM orbit number was 46791. Figs. 13 (a)-(d) depict a series of MTSAT IR observations from 2300 UTC January 30, 2006, to 0200 UTC on January 31, 2006. The target in the Taiwan Strait was not moving, except in the region from 25°N to 27°N and 121°E to 123°E (hereafter Region A). The cloud height of Region A was higher than that in the Taiwan Strait. Fig. 14 displays the

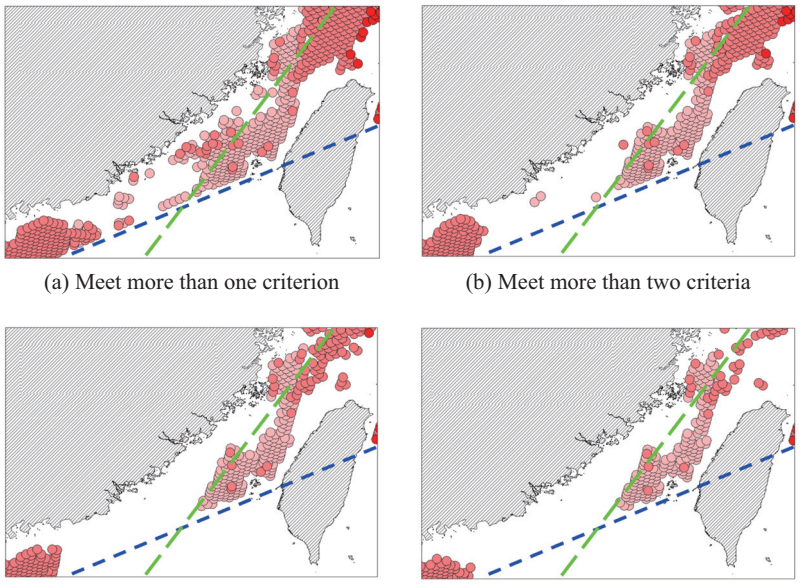

(a) Meet more than one criterion (b) Meet more than two criteria

(c) Meet more than three criteria (d) Meet four criteria

Fig. 15. Case verification at 0054 UTC on January 31, 2006. The figures meet more than (a) one, (b) two, (c) three criteria, and (d) all four criteria. Dashed line delineates the edge of swath, long dashed line represents the Taiwan Strait center line, and purple circles indicate the FOV of TMI.

VIS observation at 0100 UTC. The distribution of a high albedo is located to the east of the Taiwan Strait center line and Region A. The target in the east of the Taiwan Strait center line appears smooth in the VIS observation, whereas cloud textures are evident at the target in Region A. Figs. 13 and 14 provide a detailed analysis of the satellite observations, where the target in the east of the Taiwan Strait center line is likely to be fog, and Region A contains low clouds.

Figs. 15(a)-(c) depict the results obtained when more than one, two, and three criteria met, respectively; Fig. 15(d) depicts the outcome when all four fog criteria were satisfied. Fig. 15(a) illustrates that Region A and most of the Taiwan Strait were covered by sea fog. The green dashed line in Fig. 15 indicates the Taiwan Strait center line. The sea fog areas to the west of the Taiwan Strait center line and Region A gradually disappeared, as illustrated in Figs. 15(b)-(d). In Fig. 15, there is no circle within 20 km of the isolated islands such as that on which the Magong airport is located. This is because the high emissivity from land affected the TBs, thereby requiring data that covered areas within 20 km of land to be removed.

Although there was no ground observation for verifying whether clouds or fog was present in Region A, the VIS image illustrates that the target in the Taiwan Strait was smoother than that in Region A. In addition, the target in Region A had a textured appearance. Furthermore, the IR image indicates that the height of the target in the Taiwan Strait was lower than that in Region A. On the basis of these data, it can be inferred that the target in Region A was a cloud, and that the target in the Taiwan Strait was fog. The VIS observation indicated that the high albedo distribution in Fig. 14 was similar to the fog area distribution in Fig. 15.

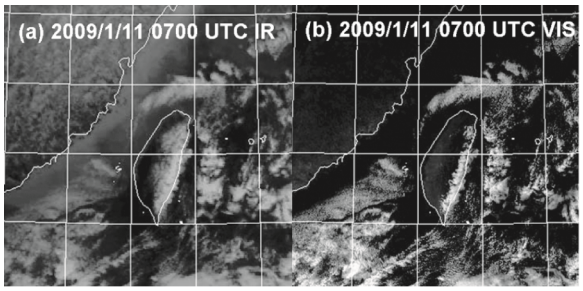

Fig. 16. (a) IR and (b) VIS observations at 0700 UTC on January 11, 2009.

The ground station observations from the Beigan airport indicated that the visibility reached 100 and 0 m, respectively, at 0000 and 0100 UTC on January 31, 2006. The observations from the Magong airport indicated that the visibility was only 600 and 1000 m, respectively, at 2330 and 2400 UTC on January 30, 2006, but 2800 m at 0100 UTC on January 31, 2006. We conclude that fog was initially present, but gradually dissipated with time. The main implication from this case is that fulfillment of at least one fog criterion indicates either low clouds or fog, as depicted in Fig. 15(a). However, fulfillment of two or more fog criteria indicates that fog existed, as shown in Figs. 15(b)-(d). These results indicate that passive microwave data can be used not only to detect sea fog but also to distinguish low clouds from fog.

2) Nonfog Cases: Clear and Cloudy Skies

The third case was a clear sky condition. The TMI scan time was 0656 UTC on January 11, 2009, and the TRMM orbit number was 63566. On that day, as depicted in Figs. 16(a) and (b),

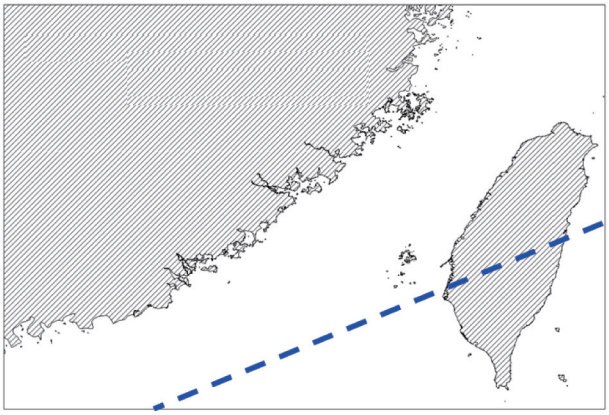

Meet more than one criterion

Fig. 17. Case verification at 0656 UTC on January 11, 2009. The figure meets more than one criterion. Dashed line indicates the edge of swath.

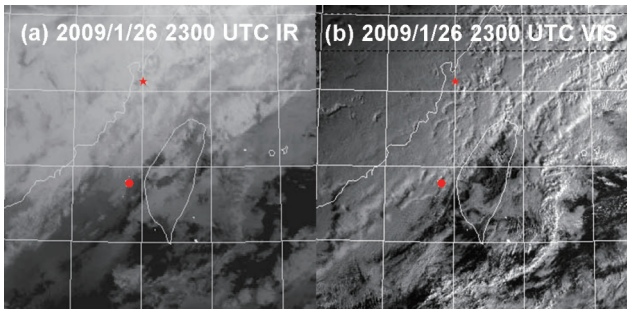

★: Beigan airport, •: Magong airport

Fig. 18. (a) IR and (b) VIS observations at 2300 UTC on January 26, 2009.

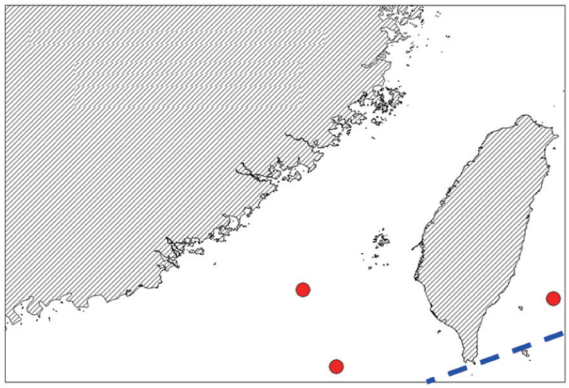

(a) Meet more than one criterion

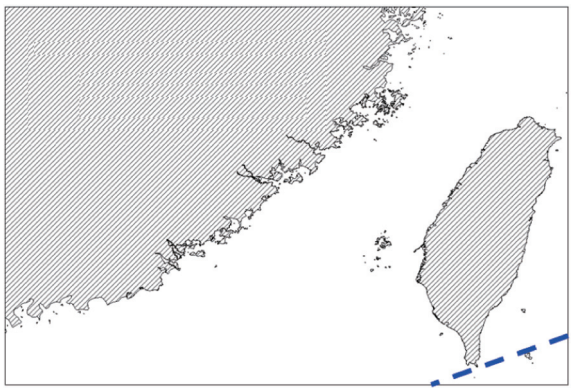

(b) Meet more than two criteria

Fig. 19. Case verification at 2243 UTC on January 26, 2009. The figures meet more than (a) one and (b) two criteria. Dashed line indicates the edge of swath, and circle represents the FOV of TMI.

the IR and VIS observations at 0700 UTC indicated some low clouds in the Taiwan Strait and higher clouds over the coastal waters north of Taiwan, while the rest of the Taiwan Strait had clear skies.

Fig. 17 depicts the outcome obtained when more than one fog criterion was met. With no indication of any sea fog in the Taiwan Strait, the same result occurred when more fog criteria were met. This is consistent with satellite observations, which indicated no fog. Evidently, our fog detection method can also be used for clear skies. The ground station observations from both the Beigan and Magong airports indicated that the visibility exceeded 9999 m during that time.

The final case was a cloudy condition. The TMI scan time was 2243 UTC on January 26, 2009, and the TRMM orbit number was 63810. The results from the IR and VIS observations performed at 2300 UTC on the same day are presented in Figs. 18(a) and (b). There were two or more levels of non-homogeneous clouds in the East China Sea and northern Taiwan Strait. In addition, low clouds or fog were evident in the southern Taiwan Strait and regions near the Magong airport.

Fig. 19(a) depicts the results obtained when more than one fog criterion was met, and Fig 19(b) shows the results obtained when more than two criteria were met. Fig. 19(a) indicates that there were only two fog points in the Taiwan Strait, whereas Fig. 19(b) indicates that there were no points. Specifically, neither Fig. 19(a) nor Fig. 19(b) shows fog areas near the Magong airport. Thus, the visibility at the Magong airport should have been higher than 1000 m at that time, even though the corresponding satellite observations indicated that there were low clouds or fog over the airport.

The actual observations from Magong airport indicated that the visibility was 9999 and 9000 m at 2200 and 2300 UTC, respectively. These visibility values were significantly higher than the values defined for fog by the WMO. Thus, it was inferred that low clouds were near the Magong airport instead of fog. Conclusive proof is thus provided that the method proposed in this study is more applicable in detecting fog than are satellite observations.

2. Quantitative Analysis

Table 3 summarizes the information on the 10 fog cases, and the fog detection efficiency is provided in Fig. 20. The horizontal axis shows the number of fog criteria that were met,

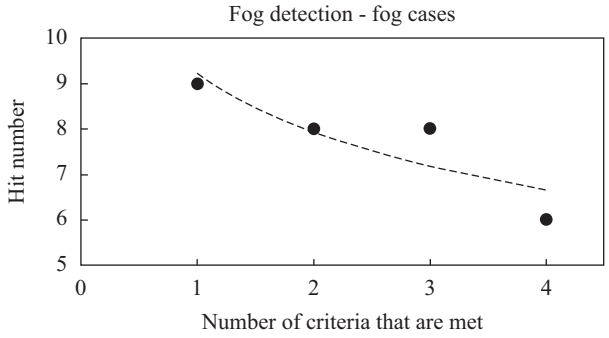

Fig. 20. Fog detection evaluation for fog cases with different criteria; dashed line represents the best fit for all points.

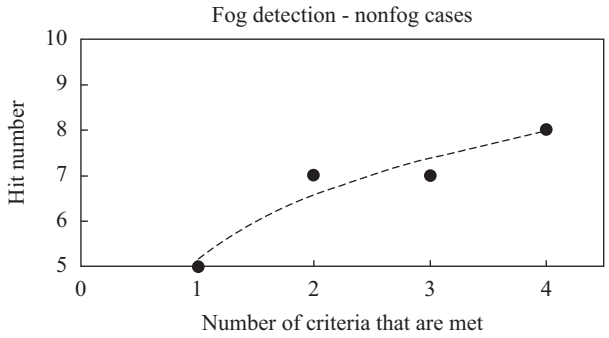

Fig. 21. Fog detection evaluation for nonfog cases with different criteria; dashed line represents the best fit for all points.

and the vertical axis indicates the hit number for the 10 fog cases. As illustrated in the graph, nine cases were estimated correctly when more than one criterion was met. As the required criteria number was increased, the hit number decreased. The hit number tended to decrease as the number of fog criteria that were met increased. This is indicated by the dashed line. Furthermore, Table 4 presents the information for the 10 nonfog cases, which involved cloudy and clear-sky conditions. Fig. 21 shows the nonfog detection accuracy. In contrast to the tendency depicted in Fig. 20, the hit number tended to increase as the number of fog criteria that were met increased.

It seemed reasonable that when the criteria limitation is increased (decreased), the hit number decreases (increased) in fog (nonfog) case detection. To facilitate applying the method to various weather conditions rather than predefined environments (fog or nonfog), Fig. 22 was plotted to define the optimal number of criteria for detecting fog. The black bar in the histogram represents a correct estimate, and the white bar represents a false positive. The greater the number of correct estimates is, the fewer the false alarms. Experiments demonstrated that the fog estimates were the most accurate when two or three fog criteria were met . In total, the accuracy of fog detection reached 75%.

In addition, the TB difference between fog and clear conditions was found to reach up to approximately 40 K and 60 K at the 37 GHz and 85 GHz horizontal polarizations. Theoretical

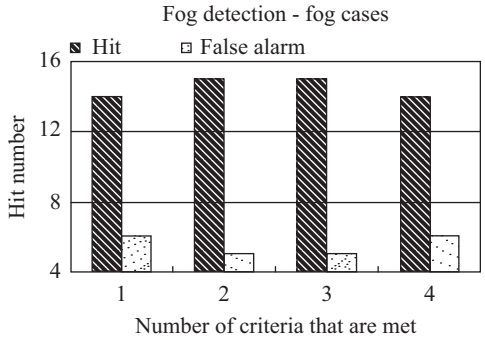

Fig. 22. Evaluation of the hits and false alarms with different criteria.

research has indicated that the slopes of the 37 GHz and 85 GHz horizontal polarizations are steeper than those of other channels before saturation. Therefore, the TB differences between fog and clear conditions at 37 GHz and 85 GHz horizontal polarizations, respectively, are the most drastic. In addition, the 85 GHz horizontal polarization TB is the most sensitive to fog.

VI. CONCLUSION AND FUTURE WORK

This study developed a new evaluation framework for fog detection by using passive microwave data. Several conclusions were drawn from the results:

(1) Microwave data can be used to detect fog over oceans during either the daytime or nighttime. By contrast, IR and VIS channels have more observation-time limitations.
(2) The accuracy of fog detection reached 75%.
(3) The 85 GHz horizontal polarization is the most sensitive to fog. The four fog criteria of the four channels are listed in Table 2.

According to the in-depth analysis, it can be concluded that passive microwave data have strong potential for detecting fog.

This study had several limitations. First, because the established criteria were tailored to conditions in the Taiwan Strait, the current fog detection mechanism can be applied only to the Taiwan Strait. Second, the time resolution of the TMI is not as high as that of a synchronous satellite, and the swath of the TMI is not fixed. Consequently, the passive microwave data cannot monitor the same area in a timely manner. Third, many atmospheric parameters can affect the microwave observations of the TMI, such as wind speed and sea surface temperature. The criteria for fog detection around the Taiwan Strait and the East China Sea were established according to winter conditions. Thus, the criteria are deemed the most suitable for the winter. Finally, when clouds are present above the fog layer, the method is less effective.

Our findings highlight the need to develop a clearer understanding of this new research topic. Some crucial directions for future research are listed as follows:

(1) More fog cases will be added to our database to improve the fog detection accuracy.
(2) Gultepe et al. (2009) demonstrated that liquid water content rises with an increasing droplet number concentration. When these two values increase, the visibility value decreases. Evidently, the liquid water content and droplet number concentration are critical elements for the visibility value and formation of fog. The purpose of considering the liquid water content and droplet number concentration is to obtain more accurate results.
(3) More channels will be used to identify the most suitable channels for fog detection.

In the future, different areas and seasons can be studied, and the criteria should be revised to account for more atmospheric parameters.

REFERENCE

Adler, R. F., C. Kidd, G. W. Petty, M. Morrissey and H. M. Goodman (2001). Intercomparison of global precipitation products: the third precipitation intercomparison project (PIP-3). Bulletin of the American Meteorological Society 82, 1377-1396.

Anthis, A. I. and A. P. Cracknell (1999). Use of satellite images for fog detection (AVHRR) and forecast of fog dissipation (METEOSAT) over lowland Thessalia, Hellas. International Journal of Remote Sensing 20, 1107-1124.

Bader, M. J., G. S. Forbes, J. R. Grant, R. B. E. Lilley and A. J. Waters (1995). Images in weather forecasting - A practical guide for interpreting satellite and radar imagery. University of Cambridge press.

Bendix, J. (2002). A satellite-based climatology of fog and low-level stratus in Germany and adjacent areas. Atmospheric Research 64, 3-18.

Bendix, J., B. Thies, T. Nauss and J. Cermak (2006). A feasibility study of daytime fog and low stratus detection with TERRA/AQUA-MODIS over land. Meteorological Applications 13, 111-125.

Cermak, J. and J. Bendix (2008). A Novel Approach to Fog/Low Stratus Detection using Meteosat 8 Data. Atmospheric Research 87, 279-292.

Cermak J. and J. Bendix (2011). Detecting ground fog from space-a microphysics-based approach. International Journal of Remote Sensing 32, 3345-3371.

Cho, Y. K., M. O. Kim and B. C. Kim (2000). Sea fog around the Korean Peninsula. Journal of Applied Meteorology 39, 2473-2479.

Eldridge, R. G. (1971). The relationship between visibility and liquid water content in fog. Journal of Atmospheric Sciences 28, 1183-1186.

Eric, D. C. and the Maryland Space Grant Consortium (1997). An Introduction to Satellite Image Interpretation, Johns Hopkins University press.

Eyre, J. R., J. L. Bownscombe and R. J. Allam (1984). Detection of fog at night using Advanced Very High Resolution Radiometer (AVHRR) imagery. Meteorological Magazine 113, 266-271.

Gao, S., W. Wu, L. L. Zhu, G. Fu and B. Huang (2009). Detection of nighttime sea fog/stratus over the Huanghai Sea using MTSAT-1R IR data. Acta Oceanologica Sinica 28, 23-35.

Greenwald, T. J. and S. A. Christopher (2000). The GOES I-M imagers: New tools for studying microphysical properties of boundary layer stratiform clouds. Bulletin of the American Meteorological Society 81, 2607-2620.

Gultepe, I., G. pearson, J. A. Milbrandt, B. Hansen, S. Platnick, P. Taylor, M. Gordon, J. P. Oakley and S. G. Cober (2009). The fog remote sensing and modeling field project. Bulletin American Meteorological Society, 90, 341-359.

Gultepe, I., R. Tardif, S. C. Michaelides, J. Cermak, A. Bott, J. Bendix, M. D. Müller, M. Pagowski, B. Hansen, G. Ellrod, W. Jacobs, G. Toth and S. G. Cober (2007a). Fog research: A review of past achievements and future perspectives. Pure and Applied Geophysics 164, 1121-1159.

Gultepe, I., M. Pagowski and J. Reid (2007b). A satellite-based fog detection scheme using screen air temperature. Weather and Forecasting 22, 444-456.

Gultepe I., T. Kuhn, M. Pavolonis, C. Calvert, J. Gurka, A. J. Heymsfield, P. S. K. Liu, B. Zhou, R. Ware, B. Ferrier, J. Milbrandt and B. Bernstein (2014). Ice fog in Arctic during FRAM–ice fog project: aviation and nowcasting applications. Bulletin American Meteorological Society, 95, 211-226.

Hamazu, K., H. Hashiguchi, T. Wakyama, T. Matsuda, R. J. Doviak and S. Fukao (2003). A 35-GHz scanning doppler radar for fog observations. Journal of Atmospheric and Oceanic Technology 20, 972-986.

Hu, J. C., W. J. Chen, C. Chiu, J. L. Wang and G. R. Liu (2009). Quantitative precipitation estimation over ocean using Bayesian approach from microwave observations during the typhoon season. Terrestrial, Atmospheric and Oceanic Sciences 20, 817-832.

Kim, C. K. and S. S. Yum (2010). Local meteorological and synoptic characteristics of fogs formed over Incheon international airport in the west coast of Korea. Advances in Atmospheric Sciences 27, 761-776.

Kim, C. K. and S. S. Yum (2011). Marine boundary layer structure for the sea fog formation off the west coast of the Korean Peninsula. Pure and Applied Geophysics 169, 1121-1135.

Lee, T. F., F. J. Turk and K. Richardson (1997). Stratus and fog products using GOES-8-9 3.9 μm data. Weather and Forecasting 12, 664-677.

Liu, X. and X. Q. Hu (2008). Sea fog automatic detection over the East China Sea using MTSAT data (in Chinese). Journal of Oceanography in Taiwan Strait 1, 112-117.

Mohan, M. and S. Payra (2009). Influence of aerosol spectrum and air pollutants on fog formation in urban environment of Megacity Delhi, India. Environmental Monitoring and Assessment 151, 265-277.

Pagowski, M., I. Gultepe and P. King (2004). Analysis and modeling of an extremely dense fog event in southern Ontario. Journal of Applied Meteorology 43, 3-16.

Petty, G W., S. A. Boukabara, N. Snell and J. L. Moncet (2001). Algorithm theoretical basis document for the conical-scanning microwave imager/sounder (CMIS) environmental data records: precipitation type and rate EDR. Atmospheric and Environmental Research, Inc.

Wang, P. K. (1997). Cloud Physics (in Chinese). Bo Hai Town Culture CO., LTD. 382.

Wang Y., S. Gao, G. Fu, J. Sun and S. Zhang (2014). Assimilating MTSAT-Derived humidity in nowcasting sea fog over the Yellow Sea. Weather and Forecasting 29, 205-225.

Wetzel, M. A., R. D. Borys and L. E. Xu (1996). Satellite microphysical retrievals for land-based fog with validation by balloon profiling. Journal of Applied Meteorology 35, 810-829.

Yoo, J. M., M. J. Jeong, Y. M. Hur and D. B. Shin (2010). Improved fog detection from satellite in the presence of clouds. Asia-Pacific Journal of Atmospheric Sciences 46, 29-40.